Title

Universal Approach to Quantum Adiabaticity via Ancilla Cavity

Permalink

https://escholarship.org/uc/item/9v43w7tx

Author

Tian, Lin

Publication Date

2020-03-15

Peer reviewed

Universal Approach to Quantum Adiabaticity via Ancilla Cavity

Lin Tian*

School of Natural Sciences, University of California, Merced, California 95343, USA

A central challenge in the successful implementation of adiabatic quantum algorithms is to maintain the quantum adiabaticity during the entire evolution. However, the energy gap between the ground and the excited states of interacting many-body systems often decreases quickly with the number of qubits, and the quantum adiabaticity can be severely impaired. Despite numerous previous efforts, a practical method to preserve the quantum adiabaticity has yet to be developed. Here we present a universal approach to enhancing the quantum adiabaticity via cavity or circuit QED. By coupling an adiabatic quantum computer to an ancilla cavity, the coupled system can exhibit a bistable regime with bifurcation points, where the time evolution becomes very slow. Utilizing these generic nonlinear features, we show that the energy gap of the adiabatic quantum computer can be positioned between the bifurcation points, which results in strongly-enhanced quantum adiabaticity. We then apply this method to a quantum two-level system, an Exact Cover problem, and a transverse field Ising model. In contrast to previous works, this approach does not require the spectral knowledge of the quantum system or the construction of unphysical interactions and can be applied to a vast variety of adiabatic quantum processes.

I. INTRODUCTION

Adiabatic quantum computing is a powerful approach to generating desired many-body states and has been intensively studied for solving computationally-hard problems, such as the NP-complete problems and adiabatic optimization [1–5]. In a typical adiabatic quantum algorithm, the system Hamiltonian H_s is tuned slowly from an initial Hamiltonian H_0 to a target Hamiltonian H_T with $H_s(t) = [1-z(t)]H_0 + z(t)H_T$, where $z(t)$ is a smooth function of the time t with $z(t) = 0$ at $t = 0$ and $z(t) = 1$ at the final time T [6]. The system is initially prepared in the ground state of H_0, and the ground state of H_T encodes the solution to the classically-intractable problem. During the time evolution, the system remains in the instantaneous ground state of $H_s(t)$ and evolves adiabatically to reach the ground state of H_T.

To implement an adiabatic quantum algorithm successfully, the adiabatic criterion needs to be satisfied during the evolution. A commonly-adopted form of the adiabatic criterion is $|dH_s(t)/dt| \ll \Delta_{gp}^2$, where $|dH_s(t)/dt|$ is the magnitude of the transition matrix elements of $dH_s(t)/dt$ and Δ_{gp} is the energy gap between the ground and the excited states [7]. In an interacting many-body system, the energy gap often decreases quickly with the number of qubits, and the adiabatic criterion can be violated [8]. The breaking of the quantum adiabaticity can induce diabatic transitions to the excited states with the system not reaching the desired ground state. For a quantum two-level system (TLS), the probability of such transitions is given by the Landau-Zener (LZ) formula [9, 10]. In dynamical quantum phase transitions, such transitions have been widely studied in terms of the Kibble-Zurek mechanism and the scaling laws [11–15].

A number of methods have been developed to preserve the quantum adiabaticity and reduce the transition to the excited states. Some approaches aim at maintaining a finite energy gap via inhomogeneous ramping or by dividing the evolution into short segment [16–21]. It was also shown that the energy gap can be enlarged by engineering the initial and the final Hamiltonian or by adding an intermediate Hamiltonian [22–26]. Spectral gap amplification has been designed in adiabatic quantum algorithms with frustration-free Hamiltonian [27]. In another method, the second-order phase transition was exploited to avoid exponentially-decreasing energy gap [28]. Other methods improve the local adiabaticity in the gap region with time-dependent ramping, including the nonlinear power-law ramping, the local adiabatic approach, and the optimal control approach [29–37]. Meanwhile, geometric approaches that seek time-optimal path to the desired state have been investigated [38, 39]. Recently, it was shown that the desired ground state can be reached by adding counter-diabatic interactions to eliminate the transition to the excited states [40–44]. However, all these approaches require either a priori knowledge of the energy spectrum of the quantum system, which is hard to obtain with classical methods, or the construction of unphysical interactions, which are challenging to implement in practical systems.

Here we present a universal approach that can strongly enhance the quantum adiabaticity via cavity or circuit quantum electrodynamics (QED), where an adiabatic quantum computer is coupled to an ancilla cavity with H_0 as the coupling operator. The cavity serves as a knob that controls the Hamiltonian of the adiabatic quantum computer, but is also influenced by the state of the quantum computer. With the intrinsic nonlinear features of the operator average $X_{ss} = \langle H_0 \rangle$ and its derivative X_{ss}', this coupled system can exhibit a bistable regime with bifurcation points, where the time evolution is very slow [45–48]. We show that the energy gap can be positioned between the bifurcation points so that the time evolution in the gap region can be significantly slowed

*Electronic address: ltian@ucmerced.edu

down. We then conduct numerical simulation of this approach on a quantum TLS, an Exact Cover (EC) problem, and a one-dimensional transverse field Ising model (TFIM). Our numerical result shows that the quantum adiabaticity can be strongly enhanced.

This approach is rooted in the generic properties of the operator average X_{ss} and its derivative X'_{ss} in adiabatic quantum computers. We find that X_{ss} increases monotonically but nonlinearly with the magnitude of H_0 in the Hamiltonian H_s, and furthermore, X'_{ss} reaches maximum in the gap region. These properties ensure the existence of a bistable regime with bifurcation points in this coupled system and make it possible to position the energy gap between the bifurcation points. More importantly, it only requires the knowledge of X_{ss} and X'_{ss} at the initial and the target Hamiltonians to choose appropriate system parameters. In contrast to previous works, this method does not require the spectral knowledge of the adiabatic quantum computer, nor does it require the engineering of unphysical interactions. This approach can hence be applied to a vast variety of adiabatic quantum processes when combined with the cavity or circuit QED technology [49–53].

This paper is organized as follows. We first present our approach in Sec. II. The generic properties of the operator average X_{ss} and its derivation $X_{ss}\prime$, the stationary state and bifurcation points, and the requirements on the system parameters will be discussed in this section. We then apply this approach to a quantum TLS, an EC problem, and a TFIM in Secs. III, IV, and V, respectively, and give the numerical result of the quantum adiabaticity for these models. In Sec. VI, we discuss the generality of this approach with different control parameters and different forms of coupling. Conclusions are given in Sec. VII.

II. ADIABATIC QUANTUM COMPUTING WITH ANCILLA CAVITY

Consider an adiabatic quantum computer coupled to an ancilla cavity. The Hamiltonian of the adiabatic quantum computer is given by

$$H_s(B_x) = -B_x H_0 - J_0 H_T, \qquad (1)$$

where B_x (J_0) is the magnitude of the Hamiltonian H_0 (H_T) with $B_x \gg J_0$. Different from previous works [1, 6], here B_x and J_0 are fixed. The Hamiltonian of the cavity in the rotating frame of the driving field is

$$H_c = -\Delta_c a^\dagger a - \epsilon(a + a^\dagger) + H_{cb}, \qquad (2)$$

where a $(a^\dagger)$ is the annihilation (creation) operator of the cavity mode, Δ_c is the detuning, ϵ is the driving amplitude, and H_{cb} is the interaction between the cavity and its bath modes [54]. We assume the bath modes induce dissipation of the cavity with a damping rate κ. Let the coupling between the adiabatic quantum computer and the cavity be $H_{int} = g(a + a^\dagger)H_0$ with a coupling

strength g. This coupling is a dipole interaction between the cavity displacement $(a + a^\dagger)$ and the Hamiltonian H_0 [55, 56], and has been widely studied in cavity and circuit QED [49, 50, 52]. The total Hamiltonian of this system is then $H_t = H_s + H_c + H_{int}$.

We write $(a+a^\dagger) = x_a + (\delta a + \delta a^\dagger)$ in terms of the average cavity displacement $x_a = \langle a+a^\dagger \rangle$ and the fluctuation δa $(\delta a^\dagger)$. Similarly, $H_0 = X + \delta H_0$ in terms of the operator average $X = \langle H_0 \rangle$ and the fluctuation δH_0. Under strong driving and dissipation, the cavity can be treated semi-classically and the mean-field approximation can be applied [57]. Under this approximation, the product of the fluctuations $g(\delta a + \delta a^\dagger)\delta H_0$ in the interaction can be neglected with

$$H_{int} \approx g x_a H_0 + g X (a + a^\dagger) - g X x_a. \qquad (3)$$

The total Hamiltonian can then be decomposed as

$$H_t \approx H_s(\widetilde{B}_x) + H_c(\widetilde{\epsilon}), \qquad (4)$$

where $H_s(\widetilde{B}_x)$ is the Hamiltonian of the adiabatic quantum computer with an effective field $\widetilde{B}_x = B_x - g x_a$, and $H_c(\widetilde{\epsilon})$ is the Hamiltonian of the ancilla cavity with an effective driving amplitude $\widetilde{\epsilon} = \epsilon - gX$. The constant term $-gXx_a$ in (3) is omitted from (4). Here the Hamiltonian $H_s(\widetilde{B}_x)$ depends on the average cavity displacement x_a and the Hamiltonian $H_c(\widetilde{\epsilon})$ depends on the operator average $X = \langle H_0 \rangle$. The dynamics of the adiabatic quantum computer is governed by the Schrödinger equation:

$$id\left|\psi_s\right\rangle/dt = H_s(\widetilde{B}_x)\left|\psi_s\right\rangle \qquad (5)$$

with $\left|\psi_s\right\rangle$ being the state of the quantum computer. And the dynamics of the cavity is governed by the Heisenberg-Langevin equation

$$d\left\langle a\right\rangle/dt = i\Delta_c\left\langle a\right\rangle - \frac{\kappa}{2}\left\langle a\right\rangle + i\widetilde{\epsilon}. \qquad (6)$$

Both stationary and dynamical behaviors of this coupled system can be obtained by solving these equations self-consistently.

A. Generic properties of X_{ss} and X'_{ss}

We define $X_{ss}(\widetilde{B}_x) = \langle\psi_G|H_0|\psi_G\rangle$ and denote $X'_{ss}(\widetilde{B}_x)$ as its derivative, where $|\psi_G\rangle$ is the ground state of the Hamiltonian $H_s(\widetilde{B}_x)$. Our approach to enhancing the quantum adiabaticity strongly relies on the generic nonlinear features of X_{ss} and X'_{ss} in adiabatic quantum computers. Below we calculate the derivative X'_{ss} using the relation $X'_{ss}(\widetilde{B}_x) = [X_{ss}(\widetilde{B}_x+\delta B_x) - X_{ss}(\widetilde{B}_x)]/\delta B_x$ with $X_{ss}(\widetilde{B}_x + \delta B_x) = \langle\psi_G^\delta|H_0|\psi_G^\delta\rangle$ and $\delta B_x \to 0$. Here $|\psi_G^\delta\rangle$ is the ground state of the Hamiltonian $H_s(\widetilde{B}_x + \delta B_x)$ and can be written as $|\psi_G^\delta\rangle = \sum c_n|\psi_n\rangle$ with $|\psi_n\rangle$ being an eigenstate of $H_s(\widetilde{B}_x)$ and c_n being an overlap coefficient. We find that $X'_{ss}(\widetilde{B}_x) = \sum_{n\neq G}(|c_n|/\delta B_x)^2[E_n-E_G]$ with
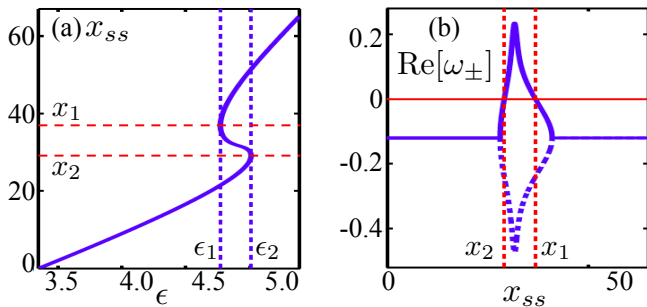
Figure 1: (a) x_{ss} vs ϵ for a TFIM of $N = 120$ qubits. (b) Re$[\omega_+]$ (solid) and Re$[\omega_-]$ (dashed) vs x_{ss}. Thin dashed lines indicate the driving amplitudes $\epsilon_{1,2}$ and the displacements $x_{1,2}$ at the bifurcation points. The parameters are $J_0 = 1$, $B_x = 1.95$, $\Delta_c = -0.14$, $\kappa = 0.12$, and $g = 0.03$.

E_n being the eigenenergy of $|\psi_n\rangle$. Assuming a finite energy gap with $(E_n - E_G) > 0$ and using the second order perturbation theory, we obtain

$$X'_{ss}(\widetilde{B}_x) = \sum_{n \neq G} \frac{|\langle \psi_n | H_0 | \psi_G \rangle|^2}{E_n - E_G}. \quad (7)$$

Therefore, $X'_{ss} > 0$ in all parameter regimes and X_{ss} increases monotonically with $\widetilde{B}_x$.

In adiabatic quantum algorithms, the eigenbasis of the Hamiltonian H_T (H_0) is typically made of eigenstates of the Pauli operators σ_{zi} (σ_{xi}) of the qubits. At $\widetilde{B}_x = 0$, $H_s = -J_0 H_T$, where the energy separation $E_n - E_G = O(J_0)$ and the matrix element $\langle \psi_n | H_0 | \psi_G \rangle \sim O(1)$ for the low-lying excited states. This analysis shows that at $\widetilde{B}_x = 0$, $X_{ss} = 0$ and $X'_{ss} = O(N)/J_0$. At $\widetilde{B}_x = B_x$ with $B_x \gg J_0$, $H_s \approx -\widetilde{B}_x H_0$, where $E_n - E_G = O(B_x)$ and $\langle \psi_n | H_0 | \psi_G \rangle \to 0$ for the low-lying excited states. We then have $X_{ss} = O(N)$ and $X'_{ss} \to 0$ at $\widetilde{B}_x = B_x$. When $\widetilde{B}_x$ is near the position of the energy gap, $\langle \psi_n | H_0 | \psi_G \rangle \sim O(1)$, but the energy separation $E_n - E_G \sim \Delta_{gp}$ for the low-lying excited states can be much smaller than J_0. From (7), we can deduce that X'_{ss} reaches maximum in the gap region. The above properties of X_{ss} and X'_{ss} are generic in adiabatic quantum computers, as confirmed by our result in Fig. 3(b) and Fig. 4(a).

B. Stationary state and bifurcation points

For given parameters with the adiabatic quantum computer in its ground state, this system can reach a stationary state with $d\langle a \rangle / dt = 0$. From (6), we derive the stationary cavity displacement as $x_{ss} = (\epsilon - gX_{ss}(\widetilde{B}_x))/\alpha$ with $\alpha = -[\Delta_c^2 + (\kappa/2)^2]/2\Delta_c$ and $\widetilde{B}_x = B_x - gx_{ss}$. Here x_{ss} and $X_{ss}(\widetilde{B}_x)$ depend mutually on each other and can be solved self-consistently. For illustration, we plot the displacement x_{ss} of a cavity coupled to a TFIM [58] vs the driving amplitude ϵ in Fig. 1(a). Details of this model

are given in Sec. V. The solution exhibits a bistable regime, where two stable and one unstable solutions exist at a given driving amplitude with the bifurcation points ϵ_1 and ϵ_2. This is a universal feature of an adiabatic quantum computer coupled to a cavity resulting from the nonlinear properties of X_{ss} and X'_{ss}.

It can be shown that $d\epsilon/dx_{ss} = \alpha - g^2 X'_{ss}(\widetilde{B}_x)$. At the bifurcation points, $d\epsilon/dx_{ss} = 0$, i.e., $X'_{ss}(\widetilde{B}_x) = \alpha/g^2$, as indicated by the thin dashed lines in Fig. 1(a). Hence, for this system to contain two bifurcation points, the parameters need to satisfy the condition $X'_{ss}(0) < \alpha/g^2 < \max[X'_{ss}]$.

The dynamics near the bifurcation points is strongly affected by the above nonlinear features. Define a small shift δx_a (δp_a) from the stationary displacement (momentum) with $x_a = x_{ss} + \delta x_a$ ($p_a = p_{ss} + \delta p_a$). Assume the adiabatic quantum computer remains in the ground state so that the operator average can be linearized as $X = X_{ss} - gX'_{ss}\delta x_a$. Using (6), we obtain

$$\frac{d}{dt}\begin{bmatrix} \delta x_a \\ \delta p_a \end{bmatrix} = \begin{bmatrix} -\kappa/2 & -\Delta_c \\ \Delta_c - 2gX'_{ss} & -\kappa/2 \end{bmatrix}\begin{bmatrix} \delta x_a \\ \delta p_a \end{bmatrix}. \quad (8)$$

The secular frequencies of the small shift are then

$$\omega_\pm = -\kappa/2 \pm \sqrt{(-2\Delta_c g^2 X'_{ss} - \Delta_c^2)}. \quad (9)$$

At the bifurcation points with $X'_{ss}(\widetilde{B}_x) = \alpha/g^2$, the real part of ω_+ approaches zero, as shown in Fig. 1(b). A vanishing real part indicates that the time evolution in the vicinity of the bifurcation points becomes very slow. During an adiabatic evolution, the quantum adiabaticity in the gap region is the most vulnerable to diabatic transitions. In our approach, using the knowledge of X_{ss} and X'_{ss} at $\widetilde{B}_x = 0$ and B_x, we can engineer the system parameters to position the energy gap between the bifurcation points so as to slow down the time evolution in this region and enhance the quantum adiabaticity.

C. Adiabatic protocol

Below we choose the driving amplitude as the control parameter in our adiabatic protocol. From the discussions in Secs. II A and II B, the parameters of this system need to satisfy the following conditions. First, $\Delta_c < 0$, i.e., $\alpha > 0$, so that the real part of the secular frequency ω_+ can reach zero. Second, $X'_{ss}(0) < \alpha/g^2 < \max(X'_{ss})$ so that there are at least two bifurcation points in the driving amplitude. Finally, $\epsilon_i < \epsilon_f$, i.e., $X_{ss}(B_x)/B_x < \alpha/g^2$, so that the system switches from the lower branch to the upper branch (or vice versa) at a bifurcation point and crosses the gap region during the switching. In addition to these conditions, the cavity damping rate κ and cavity detuning Δ_c strongly affect the dynamics of this system. They can be chosen based on the magnitudes of B_x and J_0 and on the realistic range of the parameters in a physical system. To determine the system parameters, it only requires the knowledge of X_{ss} and X'_{ss} at

$\widetilde{B}_x = 0$ and B_x, which can be obtained analytically. Our approach thus does not require the spectral knowledge of the adiabatic quantum computer or the engineering of unphysical interactions.

As a control parameter, the driving amplitude can be tuned slowly or suddenly. In both cases, the system will evolve continuously [48]. We adopt the following adiabatic protocol for our numerical simulation in Secs. III, IV, and V. The driving amplitude is initially biased at ϵ_0 with $x_{ss} = 0$ ($\widetilde{B}_x = B_x$) and the adiabatic quantum computer is in the ground state of $H_s(B_x)$. At time $t = 0$, the driving amplitude is switched to an intermediate value ϵ and the system starts evolving towards the stationary state of ϵ. For ϵ larger than a value $\epsilon_c \approx \epsilon_2$, the effective field $\widetilde{B}_x$ decreases to cross the position of the energy gap. When $\widetilde{B}_x$ is well below the gap position, the driving amplitude is tuned to ϵ_f, which corresponds to $x_{ss} = B_x/g$ ($\widetilde{B}_x = 0$). In the ideal scenario, the system then evolves towards the ground state of the Hamiltonian $-J_0 H_T$.

During the evolution, diabatic transitions to the excited states can occur, which will degrade the fidelity of the final state. The aim of our protocol is to find an ϵ that greatly reduces the probability of such transitions. Because we do not have accurate knowledge of ϵ_c (ϵ_2), the above protocol needs to be repeated a number of times to reach a desired ϵ. The effectiveness of this protocol can be characterized by the difference between the final field $\widetilde{B}_x(T)$ and the ideal value $\widetilde{B}_x = 0$, which is caused by the transitions to the excited states. In the following, we illustrate this approach with three models.

III. QUANTUM TWO-LEVEL SYSTEM

The Hamiltonian of the TLS is given by (1) with $H_T = -B_x\sigma_x/2J_0 + \sigma_z/2$ and $H_0 = \sigma_x$. Here $\sigma_{x,z}$ are the Pauli matrices of the TLS and $B_x \gg J_0$. Different from typical adiabatic quantum computers, H_0 and H_T almost share the same set of eigenstates $|\pm\rangle = (|0\rangle \pm |1\rangle)/\sqrt{2}$, where $|0\rangle$ and $|1\rangle$ are eigenstates of σ_z. The cavity Hamiltonian is (2) and the coupling between the TLS and the cavity is $H_{int} = g(a + a^\dagger)H_0$. As discussed in Sec. II, the total Hamiltonian of this system can be decomposed into the TLS Hamiltonian $H_s(\widetilde{B}_x)$ with an effective field $\widetilde{B}_x = B_x - gx_a$ and the cavity Hamiltonian $H_c(\widetilde{\epsilon})$ with an effective driving $\widetilde{\epsilon} = \epsilon - gX$ under the mean-field approximation. When $\widetilde{B}_x$ is swept from B_x to 0, the magnitude of the σ_x-component in $H_s(\widetilde{B}_x)$ is swept from $B_x/2$ to $-B_x/2$ with the magnitude of the σ_z-component unchanged. The energy gap occurs at $\widetilde{B}_x = B_x/2$, where $H_s(\widetilde{B}_x) = -J_0\sigma_z/2$ and $\Delta_{gp} = J_0$.

The ground-state average of the coupling operator H_0 can be derived as

$$X_{ss}(\widetilde{B}_x) = (2\widetilde{B}_x - B_x)/\sqrt{(2\widetilde{B}_x - B_x)^2 + J_0^2}. \quad (10)$$

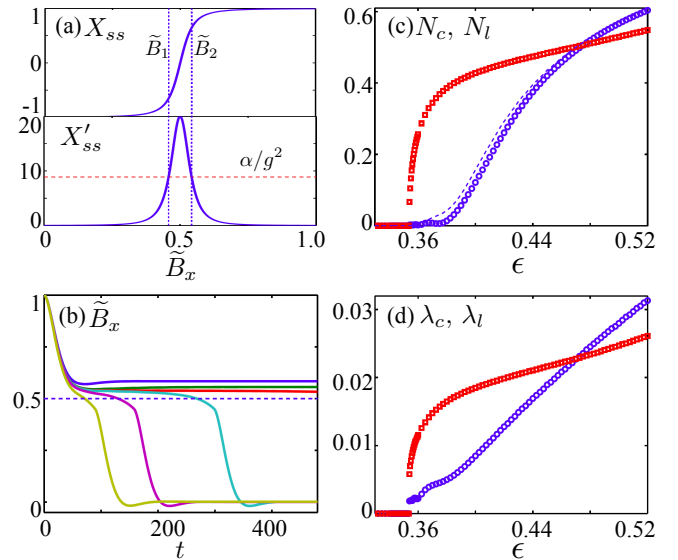At $\widetilde{B}_x = B_x$ with $B_x \gg J_0$, $X_{ss} \approx 1$ and $X'_{ss} \to 0$. At

Figure 2: (a) X_{ss} and X'_{ss} vs $\widetilde{B}_x$. Dashed lines corresponds to $X'_{ss} = \alpha/g^2$ and $\widetilde{B}_x = \widetilde{B}_{1,2}$ at the bifurcation points. (b) $\widetilde{B}_x$ vs the time t at $\epsilon = 0.34, 0.35, 0.3535, 0.354, 0.36, 0.37$ from top to bottom. The dashed line corresponds to $\widetilde{B}_x$ at the gap position. (c) N_c from the numerical simulation (circles) and the Landau-Zener formula (dashed line) and N_l in the linear-ramping model (squares) vs ϵ. (d) λ_c of the cavity-coupled TLS (circles) and λ_l of the linear-ramping model (squares) vs ϵ. Other parameters are $J_0 = 0.1$, $B_x = 1$, $\kappa = 0.1$, $\Delta_c = -0.05$, and $g = 0.075$.

$\widetilde{B}_x = 0$, $X_{ss} \approx -1$ and $X'_{ss} \to 0$. The maximum of the derivative occurs at the gap position with $\max[X'_{ss}] = 2/J_0$. Both X_{ss} and X'_{ss} are plotted in Fig. 2(a). With the requirements on the parameters discussed in Sec. II C, we choose $J_0 = 0.1$, $B_x = 1$, $\kappa = 0.1$, $\Delta_c = -0.05$, and $g = 0.075$. These parameters yield $\alpha/g^2 = 8.9$ with two bifurcation points at $\epsilon_1 = 0.31$ and $\epsilon_2 = 0.35$. The corresponding effective fields at the bifurcation points are $\widetilde{B}_1 = 0.48$ and $\widetilde{B}_2 = 0.54$. Meanwhile, at $\epsilon_0 = 0.07$, $x_{ss} = 0$ with $\widetilde{B}_x = B_x$; and at $\epsilon_f = 0.59$, the displacement reaches maximum with $x_{ss} = B_x/g$ and $\widetilde{B}_x = 0$.

We simulate the time evolution of this system numerically following the protocol outlined in Sec. II C. In Fig. 2(b), the effective field $\widetilde{B}_x$ is plotted vs the time t at several values of ϵ. For ϵ below a value $\epsilon_c \approx \epsilon_2$, $\widetilde{B}_x$ remains above the gap position $B_x/2$ during the entire evolution. For ϵ above ϵ_c, $\widetilde{B}_x$ decreases to cross the gap position. When $\widetilde{B}_x$ is below $(B_x - J_0)/2$, where the energy separation between the ground and the excited states is sufficiently large to prevent further diabatic effects, the driving amplitude is switched to ϵ_f. When ϵ approaches ϵ_c, the time evolution of the effective field in the gap region slows down significantly. Similar slowdown can be observed when the driving amplitude is switched down from ϵ_f to ϵ_0. This result indicates that the quantum adiabaticity of this process can be enhanced by choosing appropriate driving amplitude ϵ.

The quantum adiabaticity in the above process can be characterized with the ramping rate at the gap position $\lambda_c = |d\widetilde{B}_x/dt|$ [48]. For convenience of discussion, we let $\lambda_c = 0$ if $\widetilde{B}_x(t)$ does not cross the gap position. The numerical result of λ_c can be tested by estimating the probability of the TLS in the excited state with the Landau-Zener formula $N_c = \exp(-\pi\Delta_{qp}^2/2\lambda_c)$ [9, 10]. In Fig. 2(c), the estimated probability is compared with the probability obtained from the numerical simulation. The two results demonstrate excellent agreement, which verifies that λ_c is a good index to study the quantum adiabaticity in this system. As shown in Fig. 2(d), λ_c decreases significantly as ϵ approaches ϵ_c. For comparison, we define a linear-ramping model with a duration t_s and a linear-ramping rate $\lambda_l = |\widetilde{B}_x(T) - \widetilde{B}_x(0)|/t_s$, where t_s is the time in the above numerical simulation for the effective field to reach $\widetilde{B}_x(T)$ [13, 14]. Our result reveals that in a wide range of the driving amplitude ϵ, our approach outperforms the linear-ramping model with $\lambda_c < \lambda_l$ and demonstrates strongly-enhanced quantum adiabaticity. As a result, in Fig. 2(c), the excitation probability is greatly reduced with $N_c < N_l$.

IV. EXACT COVER PROBLEM

The EC problem is NP-complete and has been intensively studied in adiabatic quantum computing [1, 5]. Here we randomly generate an EC instance on $N = 6$ qubits. This instance contains $m = 5$ clauses:

$$
\begin{aligned}
C_1 &= (Q_1, Q_2, Q_5), \\
C_2 &= (Q_2, Q_3, Q_6), \\
C_3 &= (Q_3, Q_4, Q_6), \\
C_4 &= (Q_1, Q_3, Q_5), \\
C_5 &= (Q_2, Q_5, Q_6),
\end{aligned} \tag{11}
$$

where $Q_j = 0$ (1) corresponds to the eigenstate $|0\rangle$ ($|1\rangle$) of the Pauli operator σ_{zj} for the jth qubit. The clause C_i depends on the states of three qubits (Q_{i1}, Q_{i2}, Q_{i3}) and is satisfied when one and only one of these states is 1 with the other two in the state 0, i.e., $Q_{i1}+Q_{i2}+Q_{i3} = 1$. The instance in (11) has a unique solution: $Q_1 = Q_6 = 1$ and all other states are 0. The Hamiltonian that encodes the solution to this instance can be written as $H_T = \sum_i H_{Ti}$ with $H_{Ti} = \sum f_i(\vec{Q})|\vec{Q}\rangle\langle\vec{Q}|$ and $|\vec{Q}\rangle = \prod_j |Q_j\rangle$ being a product state of all qubits. Here $f_i(\vec{Q}) = 0$ if the clause C_i is satisfied and $f_i(\vec{Q}) = 1$ if C_i is violated by the state $\vec{Q}$. From this definition, $H_T = \sum f(\vec{Q})|\vec{Q}\rangle\langle\vec{Q}|$ with $f(\vec{Q})$ being the number of violated clauses by the state $\vec{Q}$. The ground state of this Hamiltonian satisfies all clauses and has $f(\vec{Q}) = 0$.

In our adiabatic protocol, the Hamiltonian of the above EC instance is given by (1), where $H_0 = \sum_j \sigma_{xj}$ with σ_{xj} being a Pauli operator of the jth qubit and $J_0 < 0$. With $B_x \gg |J_0|$, $H_s(B_x) \approx -B_x H_0$, and the ground state can
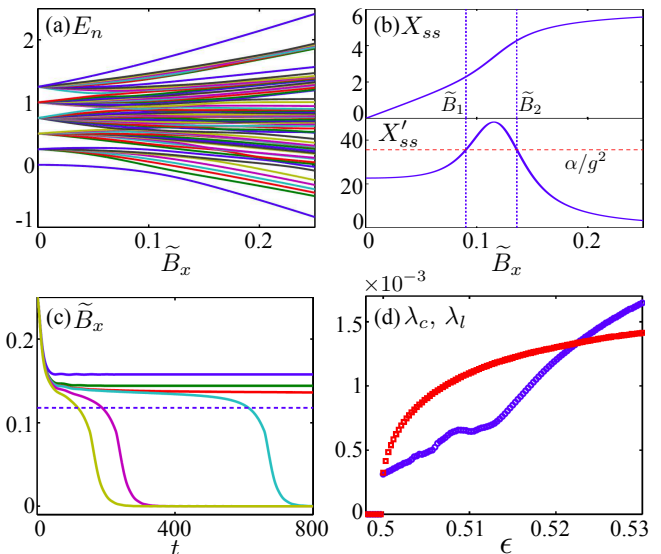

Figure 3: (a) The energy spectrum of the EC instance (11) vs $\widetilde{B}_x$. (b) X_{ss} and X'_{ss} vs $\widetilde{B}_x$. Dashed lines corresponds to $X'_{ss} = \alpha/g^2$ and $\widetilde{B}_x = \widetilde{B}_{1,2}$ at the bifurcation points. (c) $\widetilde{B}_x$ vs the time t at $\epsilon = 0.49, 0.498, 0.499, 0.5, 0.502, 0.51$ from top to bottom. The dashed line corresponds to $\widetilde{B}_x$ at the gap position. (d) λ_c of the cavity-coupled TLS (circles) and λ_l of the linear-ramping model (squares) vs ϵ. Other parameters are $J_0 = 0.25$, $B_x = 0.5$, $\kappa = 0.25$, $\Delta_c = -0.1$, and $g = 0.06$.

be approximated as $\Pi_j|+\rangle$ with all qubits in the state $|+\rangle = (|0\rangle+|1\rangle)/\sqrt{2}$. The cavity Hamiltonian is given by (2) and the qubits are coupled to the cavity via the interaction $H_{int} = g(a+a^\dagger)H_0$. The total Hamiltonian can be decomposed into the EC part $H_s(\widetilde{B}_x)$ with $\widetilde{B}_x = B_x - gx_a$ and the cavity part $H_c(\widetilde{\epsilon})$ with $\widetilde{\epsilon} = \epsilon - gX$ under the mean-field approximation, as discussed in Sec. II. Here the effective field $\widetilde{B}_x$ can be tuned continuously from B_x to 0 by varying the cavity state. The energy spectrum of $H_s(\widetilde{B}_x)$ is plotted in Fig. 3(a) for $J_0 = 0.25$ and $B_x = 0.5$. From the numerical result, we find that the energy gap is at $\widetilde{B}_x = 0.12$ with $\Delta_{gp} = 0.10$.

It can be shown that the ground-state operator average $X_{ss} = 0$ at $\widetilde{B}_x = 0$ and $X_{ss} \to N$ at $\widetilde{B}_x \gg J_0$. With a perturbation theory approach, we obtain that $X'_{ss} = 22.7$ at $B_x = 0$ and $X'_{ss} \to 0$ at $\widetilde{B}_x \gg J_0$. In Fig. 3(b), X_{ss} and X'_{ss} are plotted, which exhibit the universal features discussed in Sec. II A. We then choose the parameters for the cavity and the coupling with $\kappa = 0.25$, $\Delta_c = -0.1$, and $g = 0.06$. These parameters yield $\alpha/g^2 = 35.6$ with two bifurcation points at $\epsilon_1 = 0.48$ and $\epsilon_2 = 0.5$, respectively. Meanwhile, at $\epsilon_0 = 0.33$, $x_{ss} = 0$; and at $\epsilon_f = 0.53$, the cavity displacement reaches its maximum with $x_{ss} = B_x/g$.

Following the switching protocol described in Sec. II C, we simulate the dynamics of this coupled system by solving (5) and (6). Here the driving amplitude is switched to ϵ_f when the effective field is below 0.09. The time dependence of $\widetilde{B}_x$ is given in Fig. 3(c), which demonstrates

similar behaviors as those in Fig. 2(b). In particular, the time variation of $\widetilde{B}_x$ in the gap region significantly slows down when the driving amplitude ϵ approaches a value $\epsilon_c \approx \epsilon_2$. In Fig. 3(d), the ramping rate λ_c is plotted vs ϵ together with the linear-ramping rate λ_l defined in Sec. III. Both λ_c and λ_l decrease quickly when the driving amplitude ϵ approaches ϵ_c and $\lambda_c < \lambda_l$ in a wide range of ϵ. This result demonstrates strong enhancement of the quantum adiabaticity using our approach in comparison with the linear-ramping model.

V. TRANSVERSE FIELD ISING MODEL

The Hamiltonian of a one-dimensional TFIM can be written as (1) with $H_0 = \sum_i \sigma_{xi}$ and $H_T = \sum_i \sigma_{zi}\sigma_{zi+1}$ [58]. Here B_x is the transverse magnetic field applied to the qubits, J_0 is the ferromagnetic coupling between adjacent qubits, σ_{xi}, σ_{zi} are the Pauli operators of the ith qubit, and N is the total number of qubits in the chain. The Hamiltonian of the cavity is given by (2) and the TFIM is coupled to the cavity via the dipole interaction $H_{int} = g(a+a^\dagger)H_0$. Under the mean-field approximation, the total Hamiltonian can be decomposed into the TFIM part $H_s(\widetilde{B}_x)$ with $\widetilde{B}_x = B_x - gx_a$ and the cavity part $H_c(\widetilde{\epsilon})$ with $\widetilde{\epsilon} = \epsilon - gX$. The energy spectrum of $H_s(\widetilde{B}_x)$ is exactly solvable using the Jordan-Wigner transformation [59]. At $\widetilde{B}_x \gg J_0$ ($\widetilde{B}_x \ll J_0$), the ground state of the TFIM is in a paramagnetic (ferromagnetic) phase. The energy gap occurs at the critical point $\widetilde{B}_x = J_0$ with $\Delta_{gp} \approx 2\pi J_0/N$ for large N.

In this model, the ground-state operator average $X_{ss} = 0$ at $\widetilde{B}_x = 0$ and $X_{ss} \to N$ at $\widetilde{B}_x \gg J_0$. Using a perturbation theory approach, we find that $X'_{ss} = N/2J_0$ at $\widetilde{B}_x = 0$ and $X'_{ss} \to 0$ at $\widetilde{B}_x \gg J_0$. The maximum of X'_{ss} appears at the critical point and diverges in the thermodynamic limit. Both X_{ss} and X'_{ss} are shown in Fig. 4(a). We choose the following parameters: $B_x = 1.95$, $J_0 = 1$, $\kappa = 0.12$, $\Delta_c = -0.14$, and $g = 0.03$. These parameters yield $\alpha/g^2 = 92.1$ with two bifurcation points at $\epsilon_1 = 4.77$ and $\epsilon_2 = 5.01$, respectively. We also obtain $x_{ss} = 0$ at $\epsilon_0 = 2.23$ and the cavity displacement reaches its maximum $x_{ss} = B_x/g$ at $\epsilon_f = 5.38$.

For an initial state in the subspace of states with even number of excitations at a given effective field, the wave function of the TFIM at a time t can be written as $|\psi(t)\rangle = \prod(U_k(t) + iV_k(t)c_k^\dagger c_{-k}^\dagger)|0\rangle$ with time-dependent coefficients $U_k(t)$ and $V_k(t)$. Here $k = (2m-1)\pi/N$ with $1 \le m \le N/2$, c_k ($c_k^\dagger$) is the annihilation (creation) operator of a fermionic particle at the quasimomentum k, and $|0\rangle$ is the vacuum state [15]. The time evolution of $|\psi(t)\rangle$ is governed by (5), which can be converted to

$$i \begin{pmatrix} \dot{\bar{U}}_k \\ \dot{\bar{V}}_k \end{pmatrix} = \begin{pmatrix} -\varepsilon_k \cos 2\theta_k & -\varepsilon_k \sin 2\theta_k \\ -\varepsilon_k \sin 2\theta_k & +\varepsilon_k \cos 2\theta_k \end{pmatrix} \begin{pmatrix} \bar{U}_k \\ \bar{V}_k \end{pmatrix} \quad (12)$$

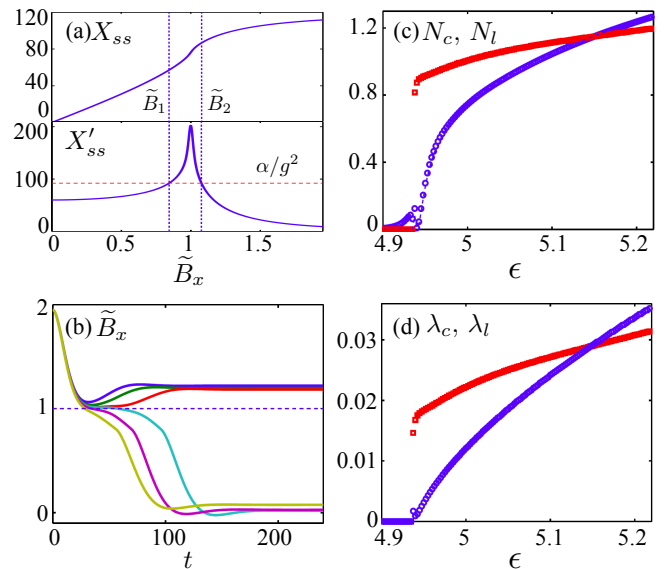in the subspace of the quasimomenta $\pm k$. Here $\bar{U}_k =$

Figure 4: (a) X_{ss} and X'_{ss} vs $\widetilde{B}_x$. Dashed lines corresponds to $X'_{ss} = \alpha/g^2$ and $\widetilde{B}_x = \widetilde{B}_{1,2}$ at the bifurcation points. (b) $\widetilde{B}_x$ vs the time t at $\epsilon = 4.90, 4.92, 4.935, 4.938, 4.95, 4.97$ from top to bottom. The dashed line corresponds to $\widetilde{B}_x$ at the gap position. (c) N_c from the numerical simulation (circles) and the Landau-Zener formula (dashed line) and N_l in the linear-ramping model (squares) vs ϵ. (d) λ_c of the cavity-coupled TLS (circles) and λ_l of the linear-ramping model (squares) vs ϵ. Other parameters are the same as those in Fig. 1.

$U_k e^{i\theta_k}$, $\bar{V}_k = V_k e^{i\theta_k}$, θ_k is an overall phase factor, and $\varepsilon_k = 2(J_0^2 + \widetilde{B}_x^2 - 2\widetilde{B}_x J_0 \cos k)^{1/2}$ is the quasiparticle energy for the time-dependent effective field $\widetilde{B}_x$. The dynamics of this system can be obtained by solving (6) and (12) self-consistently.

Under the adiabatic protocol given in Sec. II C, we simulate the time evolution of this system numerically. During the evolution, the driving amplitude is tuned to ϵ_f when the effective field decreases below $\widetilde{B}_x = 0.8$. The time dependence of $\widetilde{B}_x$ is plotted in Fig. 4(b) for several driving amplitudes, which exhibits similar behaviors to that in Fig. 2(b) and Fig. 3(c). When ϵ approaches a value $\epsilon_c \approx \epsilon_2$, the time variation of $\widetilde{B}_x$ in the gap region becomes very slow. The probability of excitation can be defined as $N_c = \sum_{k>0} |\beta_k|^2$, where β_k is the probability amplitude of the excited state in the $\pm k$ subspace [60]. In Fig. 4(c), N_c is plotted vs the driving amplitude ϵ. As ϵ approaches ϵ_c, N_c decreases accordingly. The corresponding probability of excitation N_l in the linear-ramping model defined in Sec. III also decreases, but $N_c < N_l$ in a wide range of ϵ. In Fig. 4(d), the ramping rate λ_c is plotted together with the linear-ramping rate λ_l. With $\epsilon \to \epsilon_c$, both λ_c and λ_l decrease quickly with $\lambda_c < \lambda_l$ in a wide range of ϵ. This numerical result agrees with our analysis in Sec. II C and reveals that the quantum adiabaticity can be strongly enhanced by choosing appropriate control parameters.
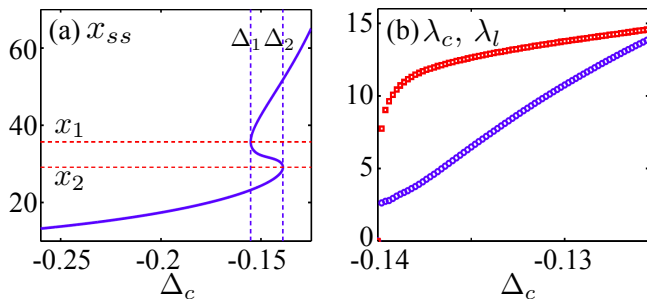
Figure 5: (a) x_{ss} vs Δ_c for a TFIM of $N = 120$ qubits. Thin dashed lines indicate the detunings $\Delta_{1,2}$ and the displacements $x_{1,2}$ at the bifurcation points. (b) λ_c of the cavity-coupled TFIM (circles) and λ_l of the linear-ramping model (squares) vs Δ_c. Here $\epsilon = 5$ and other parameters are the same as those in Fig. 1.

VI. DISCUSSIONS

As an approach that exploits time-dependent ramping to maintain the quantum adiabaticity, the advantage of our approach is that it does not require the spectral knowledge of the quantum many-body system. Instead, this method relies on nonlinear properties that are generic in adiabatic quantum computers to achieve strong enhancement of the quantum adiabaticity. It only requires the knowledge of the operator average X_{ss} and its derivative X'_{ss} at $\widetilde{B}_x = 0$ and B_x, which can be obtained analytically with perturbation theory, to engineer the system parameters. In contrast, previous works with time-dependent ramping require the spectrum knowledge of the quantum system to design the ramping rate, which is manipulated according to the local energy separation between the ground and the excited states [29–37]. Whereas the energy spectrum for questions of interest to adiabatic quantum computing is hard to obtain with classical methods.

Our approach can be applied to a wide variety of quantum systems with different control parameters and different forms of coupling. In previous sections, we use the driving amplitude as the control parameter. Other parameters can also be utilized as a control knob, such as the detuning Δ_c. For a TFIM biased at $\epsilon = 5$ with other parameters being the same as those in Fig. 1, a bistable regime in the detuning exists with two bifurcation points at $\Delta_1 = -0.155$ and $\Delta_2 = -0.14$, respectively. The stationary cavity displacement x_{ss} is plotted vs Δ_c in Fig. 5(a). Consider an adiabatic protocol, where the de-

tuning is switched from its initial value to an intermediate value Δ_c at the time $t = 0$, and then the system starts evolving towards the stationary state of Δ_c. When the effective field is below $\widetilde{B}_x = 0.8$ during the evolution, the detuning is switched from Δ_c to a final value that corresponds to $\widetilde{B}_x = 0$ in the stationary state. We conduct numerical simulation under this protocol. In Fig. 5(b), the ramping rate λ_c at the critical point is shown together with the linear-ramping rate λ_l defined in Sec. III. Strong enhancement of the quantum adiabaticity in comparison with the linear-ramping model can be observed.

Furthermore, other forms of coupling can be utilized to implement our approach as well. One example is the photon-number coupling $H_{int} = ga^\dagger a \sigma_{xi}$. In [46], it was shown that bistable behavior can be observed with this coupling. Our numerical study finds that the quantum adiabaticity can be enhanced with this interaction.

VII. CONCLUSIONS

To conclude, we studied a universal approach to enhancing the quantum adiabaticity in continuous quantum processes by coupling an adiabatic quantum computer to an ancilla cavity. This approach exploits the nonlinear features that are generic to adiabatic quantum computers to engineer the system parameters and position the gap region between the bifurcation points. The time evolution in the gap region can be significantly slowed down and the quantum adiabaticity can be strongly enhanced. We applied this method to a quantum TLS, a randomly-generated instance of the EC problem, and a TFIM using numerical simulation. The advantage of this method compared with previous methods is that it does not require the spectral knowledge of the adiabatic quantum computer or the engineering of unphysical interactions. This approach can be applied to a vast variety of adiabatic quantum processes when combined with the cavity or circuit QED technology.

[1] E. Farhi, J. Goldstone, S. Gutmann, J. Lapan, A. Lundgren, and D. Preda, Science **292**, 472 (2001).

[2] T. Kadowaki and H. Nishimori, Phys. Rev. E **58**, 5355 (1998).

[3] G. E. Santoro, R. Martoná̈k, E. Tosatti, and R. Car, Science **295**, 2427 (2002).

[4] S. Boixo, T. F. Rønnow, S. V. Isakov, Z. Wang, D. Wecker, D. A. Lidar, J. M. Martinis, and M. Troyer, Nat. Phys.**10**, 218 (2014).

[5] T. Albash and D. A. Lidar, arXiv:1611.04471.

[6] E. Farhi, J. Goldstone, S. Gutmann, and M. Sipser, arXiv:quant-ph/0001106.

[7] M. H. S. Amin, Phys. Rev. Lett. **102**, 220401 (2009).
[8] V. Murg and J. I. Cirac, Phys. Rev. A **69**, 042320 (2004).
[9] L. D. Landau, Phys. Z. Sowjetunion **2**, 46 (1932).
[10] C. Zener, Proc. R. Soc. London, Ser. A **137**, 696 (1932).
[11] J. Dziarmaga, Adv. Phys. **59**, 1063 (2010).
[12] A. Polkovnikov, K. Sengupta, A. Silva, and M. Vengalattore, Rev. Mod. Phys. **83**, 863 (2011).
[13] W. H. Zurek, U. Dorner, and P. Zoller, Phys. Rev. Lett. **95**, 105701 (2005).
[14] A. Polkovnikov, Phys. Rev. B **72**, 161201 (2005).
[15] J. Dziarmaga, Phys. Rev. Lett. **95**, 245701 (2005).
[16] G. Schaller, Phys. Rev. A **78**, 032328 (2008).
[17] E. Farhi, J. Goldstone, and S. Gutmann, arXiv:quant-ph/0208135.
[18] W. H. Zurek and U. Dorner, Phil. Trans. R. Soc. A **366**, 2953 (2008).
[19] J. Dziarmaga and M. M Rams, New J. Phys. **12**, 055007 (2010).
[20] A. del Campo, G. De Chiara, G. Morigi, M. B. Plenio, and A. Retzker, Phys. Rev. Lett. **105**, 075701 (2010).
[21] M. Collura and D. Karevski, Phys. Rev. Lett. **104**, 200601 (2010).
[22] N. G. Dickson and M. H. S. Amin, Phys. Rev. Lett. **106**, 050502 (2011).
[23] A. Perdomo-Ortiz, S. E. Venegas-Andraca, and A. Aspuru-Guzik, Quantum Info. Processing **10**, 33 (2011).
[24] E. Farhi, J. Goldstone, D. Gosset, S. Gutmann, H. B. Meyer, and P. Shor, Quantum Info. Comput. **11**, 181 (2011).
[25] V. Choi, Proc. Natl. Acad. Sci. U.S.A. **108**, E19 (2011).
[26] L. Zeng, J. Zhang, and M. Sarovar, J. Phys. A **49**, 165305 (2016).
[27] R. Somma and S. Boixo SIAM J. Comput. **42**, 593 (2013).
[28] R. Schützhold and G. Schaller, Phys. Rev. A **74**, 060304(R) (2006).
[29] D. Sen, K. Sengupta, and S. Mondal, Phys. Rev. Lett. **101**, 016806 (2008).
[30] S. Mondal, K. Sengupta, and D. Sen, Phys. Rev. B **79**, 045128 (2009).
[31] R. Barankov and A. Polkovnikov, Phys. Rev. Lett. **101**, 076801 (2008).
[32] J. Roland and N. J. Cerf, Phys. Rev. A **65**, 042308 (2002).
[33] H. T. Quan and W. H. Zurek, New J. Phys. **12**, 093025 (2010).
[34] P. Doria, T. Calarco, and S. Montangero, Phys. Rev. Lett. **106**, 190501 (2011).
[35] A. Rahmani and C. Chamon, Phys. Rev. Lett. **107**, 016402 (2011).
[36] M. J. M. Power and G. De Chiara, Phys. Rev. B **88**, 214106 (2013).
[37] N. Wu, A. Nanduri, and H. Rabitz, Phys. Rev. B **91**, 041115(R) (2015).
[38] A. T. Rezakhani, W.-J. Kuo, A. Hamma, D. A. Lidar, and P. Zanardi, Phys. Rev. Lett. **103**, 080502 (2009).
[39] P. R. Zulkowski and M. R. DeWeese Phys. Rev. E **92**, 032113 (2015).
[40] X. Chen, I. Lizuain, A. Ruschhaupt, D. Guéry-Odelin, and J. G. Muga, Phys. Rev. Lett. **105**, 123003 (2010).
[41] A. del Campo, M. M. Rams, and W. H. Zurek, Phys. Rev. Lett. **109**, 115703 (2012).
[42] S. Deffner, C. Jarzynski, and A. del Campo, Phys. Rev. X **4**, 021013 (2014).
[43] B. Damski, J. Stat. Mech. **2014**, P12019 (2014).
[44] S. Muthukrishnan, T. Albash, and D. A. Lidar, Phys. Rev. X **6**, 031010 (2016).
[45] P. G. Drazin, *Nonlinear Systems* (Cambridge University Press, Cambridge, England, 1992).
[46] L. Tian, Phys. Rev. Lett. **105**, 167001 (2010).
[47] X.-W. Luo, Y.-N. Zhang, X. Zhou, G.-C. Guo, and Z.-W. Zhou, Phys. Rev. A **94**, 053809 (2016).
[48] L. Tian, Phys. Rev. A **93**, 043850 (2016).
[49] S. M. Girvin, in Lecture Notes on *Strong Light-Matter Coupling: from Atoms to Solid-State Systems* (World Scientific, Singapore, 2013).
[50] J. Q. You and F. Nori, Nature (London) **474**, 589 (2011).
[51] M. H. Devoret and R. J. Schoelkopf, Science **339**, 1169 (2013).
[52] J. M. Raimond, M. Brune, and S. Haroche, Rev. Mod. Phys. **73**, 565 (2001).
[53] T. Langen, R. Geiger, and J. Schmiedmayer, Annu. Rev. Condens. Matter Phys. **6**, 201 (2015).
[54] L. Tian and R. W. Simmonds, Phys. Rev. Lett. **99**, 137002 (2007)
[55] The coupling Hamiltonian H_{int} is in the rotating frame of the driving frequency ω_d. The interaction in the lab frame is $H_{int}^{(0)} = 2g\cos(\omega_d t)(\hat{a} + \hat{a}^+)\sum_i \sigma_{xi}$.
[56] J. Xue, K. Seo, L. Tian, and T. Xiang, Phys. Rev. B **96**, 174502 (2017).
[57] T. Mori, J. Stat. Mech. Theo. Exp. **2013**, P06005 (2013).
[58] S. Sachdev, *Quantum Phase Transitions* (Cambridge University Press, Cambridge, England, 1999).
[59] P. Jordan and E. Wigner, Z. Phys. **47**, 631 (1928).
[60] The wave function of the TFIM can also be written as $|\psi(t)\rangle = \prod_{k>0}[\alpha_k(t) + i\beta_k(t)\gamma_k^\dagger \gamma_{-k}^\dagger]|G_k\rangle$, where γ_k ($\gamma_k^\dagger$) is the annihilation (creation) operator of the quasiparticle with the quasimomentum k, α_k (β_k) is the probability amplitude of the ground (excited) state, and $|G_k\rangle$ is the ground state in the subspace of the quasimomenta $\pm k$.